Interference of the surface plasmon polaritons with an Ag waveguide probed by dual-probe scanning near-field optical microscopy

R. Fujimoto[a], A. Kaneta[a], K. Okamoto[a, b], M. Funato[a], and Y. Kawakami[a,*]

[a] *Department of Electronic Science and Engineering, Kyoto University, Kyoto 615-8510, Japan*

[b] *Institute for Materials Chemistry and Engineering, Kyushu University, 6-10-1 Hakozaki, Higashi-ku, Fukuoka 812-8581, Japan*

∗ Corresponding author. Tel.: +81 753832310. Fax: +81 753832312.

E-mail address: kawakami@kuee.kyoto-u.ac.jp (Y. Kawakami)

ABSTRACT

The propagation of surface plasmon polaritons (SPPs) on Ag waveguides with two different widths are directly observed using dual-probe scanning near-field optical microscopy (DSNOM). We find that the waveguide structure strongly affects the propagation of locally excited SPPs. SPPs in a flat plane structure spread radially, whereas SPPs in a $3.4-\mu m$ wide waveguide structure form two-dimensional interference fringes due to the multiple reflections at the side edges. The experimental results agree well with finite-difference time-domain calculations. The results suggest that the DSNOM technique can visualize the nanoscale characteristics of the SPP waves in various plasmonic waveguides.

Keywords

Surface plasmon polaritons; Dual-probe scanning near-field optical microscope; Interferences; Finite-difference time-domain calculations

1. Introduction

Surface plasmons (SPs) are plasma oscillations of free electrons bound to the interface between a dielectric material and a metal. The SPs include the electromagnetic mode called SP polaritons (SPPs) and can interact directly with photons. The most attractive characteristic of the SPPs is their larger wave vector than that of light in free space. It enables us to miniaturize waveguide structures beyond the conventional diffraction limit. Concurrently, this feature of the SPPs requires special experimental arrangements for coupling photons with SPPs, such as an attenuated total reflection[1, 2] and a scanning near-field optical microscope (SNOM)[3, 4]. In recent studies, two configurations have been widely used to assess SPP propagations: one is a far-field excitation and a near-field detection[5, 6], and the other is a near-field excitation and a far-field detection[3, 4]. However, far-field excitation hinders local access to nanoscale structures, and far-field detection suffers from a low spatial resolution. Therefore, both near-field excitation and near-field detection of SPPs are needed for the in-depth assessment of SPP propagation. Recently, SPPs guided on an Au metal waveguide have been observed by using a dual-probe

SNOM (DSNOM) technique[7, 8], where two probes are used for the near-field excitation and detection, respectively. However, in this technique, in order to avoid a mechanical contact between the two probes, the detection probe monitors the topography and stops its scan when the illumination probe is imaged. Therefore, it is difficult to precisely estimate the distance between the two probes, particularly when the surface is rough.

Quite recently we developed a new DSNOM system[9] with a novel distance control technique, which can independently control the sample-probe distance and the probe-probe distance, combined with a dual-band modulation (DBM) technique. The distance control between the sample and the probe was achieved by adjusting the position of the sample stage to keep the oscillation voltage of the tuning fork (resonant frequency: 32 kHz) attached to the probe constant. At the same time, the distance control between the two probes was achieved by detecting the modulation signal of the detection probe, which was mechanically oscillating at a frequency of 100 Hz. The DBM technique enables the two distances to be controlled independently and enables the two probes to approach each other to within a few tens of nanometers. We have already visualized the anisotropic in-plane diffusion of carriers in an InGaN/GaN single quantum well[9]. Our version of DSNOM is a very powerful tool to investigate the detailed SPP propagation. For instance, it is applicable for the direct identification of the edge effects occurring at the waveguide edges, which were well discussed in ref. 10. Furthermore, the propagation properties at a high frequency close to the SPP resonance can be measured. The reason of this is that such frequency cannot be reached by conventional techniques, because the wave vector around the resonance is large, and in turn, closer approach to the excitation position is required.

In this paper, we assess the SPP propagation properties on two Ag structures, namely an Ag plane and an Ag waveguide, using our DSNOM system. Ag is more appropriate than Au as a waveguide material for SPPs because of its longer propagation length, as quantitatively estimated in section 3 below. The longer propagation for an Ag structure may cause SPP propagation different from that on an Au waveguide[7]. Based on finite-difference time-domain (FDTD) simulations, we estimated SPP propagation lengths and propagation properties as a function of distance from an excitation position. Comparing calculated results with experimental results, we found an interference effect in SPP propagations for a waveguide structure.

2. Experimental setup

The experimental setup of the DSNOM is illustrated in Fig. 1. Pencil-shaped fiber probes with a 40-degree cone angle were coated with Ni, Au, and Al with 10, 25, and 50 nm, respectively. An aperture with a diameter of 200 nm was then formed by pounding. The excitation and the detection probes were tilted in opposite directions at 30 degrees, so that the two probes come as close as possible without degrading excitation and detection efficiencies. We used an InGaN laser diode ($\lambda = 405$ nm in vacuum) as the excitation source. SPPs were locally excited by a near-field light localized at the tip of the

excitation probe. The SPPs propagated along the surface and were detected by a photo diode and a lock-in amplifier through the detection probe. The excitation probe kept illuminating the same position, and the detection probe scanned around it and observed propagating SPPs.

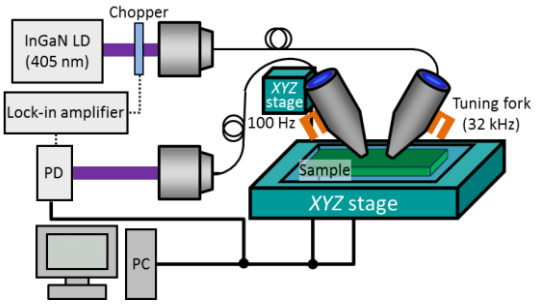

Fig. 1. (Color) Schematic image of the DSNOM system. Two *XYZ*-axis piezoelectric actuators are attached to the sample and the detection probe for scanning.

The Ag waveguide structure on a glass substrate was fabricated by conventional photolithography and lift-off. The surface images of the plasmonic waveguide are shown in Fig. 2. Figure 2(a) shows a scanning electron microscope (SEM) image of several waveguide structures with different lengths and widths, connected to a large $200 \times 200\ \mu m^2$ homogeneous thin film. We measured SPP propagation for the two structures surrounded by dotted circles: (A) is the plane structure with a width much longer than a SPP propagation length, and (B) is the waveguide structure with a $3.4 - \mu m$ width. Figure 2(b) shows an atomic force microscope (AFM) image acquired close to the center of the Ag plate in Fig. 2(a). The measured root mean square roughness, δ, was determined to be 3.76 nm from the AFM image.

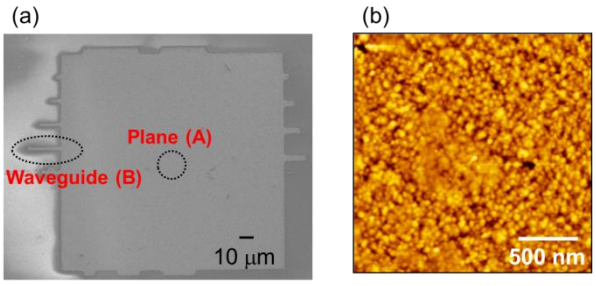

Fig. 2. (Color) Surface images of the waveguide structure. (a) SEM image with the plane (A) and the waveguide (B) structures. (b) AFM image close to the center of (a).

If a metal film inserted between two dielectric materials is sufficiently thin, two SPP modes arising at the top and the bottom interfaces couple and create two different modes, namely a symmetric mode (S mode) and an asymmetric one (AS mode)[11, 12]. The critical thickness to form these modes depends on the penetration length of the SPPs' electromagnetic field into the metal. The penetration length of the SPPs, *d*, is given by

$$d = \frac{c}{\omega}\sqrt{\left(\frac{\varepsilon_m+\varepsilon_d}{-\varepsilon_m^2}\right)} \quad (1)$$

where ε_m and ε_d are relative permittivities of the metal and dielectric, respectively, ω is the frequency of the SPP, and c is the speed of light. Here we ignore the imaginary part in the complex relative permittivity of a metal. The relative permittivity of Ag is $\varepsilon_1 = -4.41$[13] at $\lambda = 405$ nm, and the relative permittivities of the top and the bottom dielectric materials are $\varepsilon_2 = 1$ (air) and $\varepsilon_3 = 2.426$ (glass), respectively. We then acquire the critical thickness for our waveguide structure from eq. (1) to be $d = 24.7\ \text{nm(Ag/glass)} + 27.0\ \text{nm(Ag/air)} = 51.7$ nm. The wave vector of the AS mode is smaller than that of the light line in the adjacent dielectric with a larger relative permittivity. This makes the AS mode radiative, which attenuates the electric field intensity of the laterally propagating SPPs[12]. To prevent the two modes from being created, we designed a 160-nm-thick Ag film.

3. FDTD calculations

We performed three-dimensional FDTD (Poynting for Optics, FUJITSU) calculations in order to estimate SPP propagation lengths. The structure used in the simulation is shown in Fig. 3. The thickness of an Ag film was set at 100 nm, which is above the critical thickness. A 100-nm-diameter disk-shaped source with a random polarization at 405 nm is set 10 nm above the top surface (+z direction) for exciting SPPs at the interface between air and Ag. The pseudo-random polarization was made by the superposition of the linear polarizations rotated every 45 degrees in the *xy* plane. SPP propagation properties were evaluated for two structures — an Ag plane with an infinite width and a $3.4 - \mu\text{m}$ wide Ag waveguide. Each structure has infinite length in the waveguide (*x*) direction. The spatial distribution of the electric field intensity was calculated in the *xy* plane 10 nm above the top surface. A non-uniform grid was applied with a mesh size of 2.5 nm in the vicinity of the light source and 20 nm away from it. Perfect matched layer boundary conditions were used at the three boundaries.

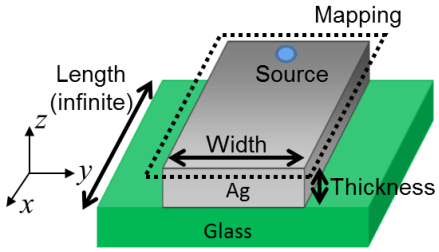

Fig. 3. (Color) The geometry of the FDTD calculation with a randomly polarized light source. The light source is located 10 nm above the Ag surface, and the electric field intensity mapping is acquired at the same height.

Given that the dielectric function of a metal is $\varepsilon_m(\omega) = \varepsilon_m'(\omega) + \mathrm{i}\varepsilon_m''(\omega)$ at an excitation frequency ω, the *x*-component of the wave vector of the SPPs, k_{SPP}, can be described by

$$k_{SPP} = k_{SPP}' + \mathrm{i}k_{SPP}''$$

$$= \frac{\omega}{c}\sqrt{\frac{\varepsilon_m \varepsilon_d}{\varepsilon_m + \varepsilon_d}} \quad (2)$$

For an Ag plane, an electric field distribution of the SPPs excited by the light source with a smaller diameter than the wavelength of light follows the cylindrical wave equation:

$$\boldsymbol{E} = \frac{\boldsymbol{E_0}}{\sqrt{\boldsymbol{r}}}\exp(\mathrm{i}\boldsymbol{k}\cdot\boldsymbol{r}) \quad (3)$$

where r is the distance from the light source. The detected light intensity in the x direction is proportional to the electric field intensity as follows:

$$E_x^2 = \frac{E_{0x}^2}{x}\exp(-2k_{SPP}^{"}x) \quad (4)$$

Therefore, the locally excited SPPs are damped due to not only the imaginary part of the wave vector, but also radial SPP propagation. The relative permittivities of Ag were reported in refs. 13-18. The two parameters in ref. 13 and ref. 14 were commonly used in other wavelength regions for calculations, and the former is known to account well for experimental results [7, 19]. We compare the reported relative permittivities of Ag and Au films at our excitation wavelength in Table 1 [13-18]. The comparison of the decay length ($l = 1/2k_{SPP}^{"}$) calculated from each relative permittivity suggests that the propagation length of SPPs in Ag is one order of magnitude larger than that in Au for the same excitation wavelength. Among the various reported values, we examined two extreme values giving the shortest (ref. 14) and the longest (ref. 13) propagation lengths for FDTD calculations.

Table 1 Dielectric constants and decay lengths of an Ag and an Au films (λ = 405 nm) according to refs. 13-18.

Reference	ε, Ag	l (μm), Ag	ε, Au	l (μm), Au
13	-4.41+0.21i	4.06	-1.70+5.75i	0.381
14	-4.01+0.70i	1.01	-1.11+6.46i	0.418
15	-4.25+0.30i	2.61	NA	NA
16, 17	-3.72+0.29i	1.94	NA	NA
18	-4.34+0.35i	2.37	-0.97+6.07i	0.392

Figures 4(a)-(d) show the normalized electric field intensity mappings. The size of each mapping is $4.0 \times 4.0\ \mu m^2$. In Fig. 4, (a) and (b) were calculated using the dielectric constant in ref. 14, and (c) and (d) — that in ref. 13. While Figs. 4(a) and (c) contain the results for the Ag plane, Figs. 4(b) and (d) are for the Ag waveguide. The solid circle at the top edge of each mapping indicates the excitation position. The dashed black lines in Figs. 4(a)-(d) are the limits of the measurable areas, which are deduced from the experimental conditions. Therefore, the non-measurable regions are excluded from the color contrast representing the intensity distribution (white regions).

Regardless of the parameters used, SPPs spread radially for the planar structure, while fringes are formed for the waveguide structure. In the waveguide structure, the SPPs interfere with the waves reflected at the side edges (solid white lines in Figs. 4(b) and (d)). Moreover, we found that the relative

permittivity in ref. 13 gives a larger difference in contrasts of the mappings between two structures, than that in ref. 14. This is because *l* with the former parameter is comparable to the waveguide width and is large enough to cause significant interference.

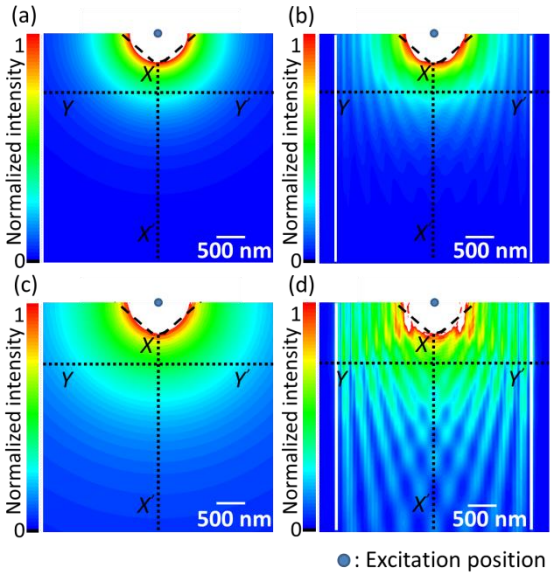

Fig. 4. (Color) Normalized electric field intensity mappings with two different dielectric constants for two structures. (a) Ag plane (ref. 14), (b) Ag waveguide (ref. 14), (c) Ag plane (ref. 13), and (d) Ag waveguide (ref. 13).

4. Results and discussion

We measured SPP propagation for the planar and waveguide structures: A and B shown in Fig. 1(a). The excitation probe remained at the excitation position, and the two-dimensional light intensity mappings were obtained using the detection probe scanning around the excitation probe. Figures 5(a) and (b) show the normalized light intensity mappings for the plane and the waveguide, respectively. The scan areas of these figures are $2.1 \times 3.2\ \mu m^2$ and $3.0 \times 4.0\ \mu m^2$, respectively. One pixel size in each mapping is $50 \times 50\ nm^2$.

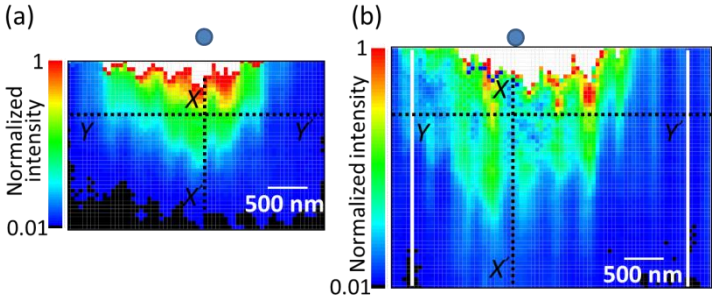

Fig. 5. (Color) Normalized light intensity mappings for the (a) Ag plane and (b) Ag waveguide.

The white regions in Figs. 5(a) and (b) show the shadows of the excitation probe, that is, the regions which we are unable to measure due to geometric considerations. They correspond to the dashed black lines in Figs. 4(a)-(d). The solid white lines in Fig. 5(b) indicate the side edges of the Ag waveguide suggested by the topographic image obtained simultaneously with the measurement. We thereby confirm that the SPPs propagate along the waveguide structure.

By comparing Figs. 5(a) and (b), we can determine the effects of the interference. As we can see from the calculation using the dielectric constant in ref. 13, the difference in the SPP propagations between the two structures is large. The periodic changes in the intensity distributions are also seen only in the waveguide. Therefore, in agreement with other reports, we deduce that the dielectric constant in ref. 13 accounts better for SPP propagation.

For a more detailed investigation of the intensity distributions, we have compared the intensity profiles along the *x* and *y* directions (dotted black lines in Figs. 4(a)-(d) and 5(a)-(b)). Figures 6(a) and (b) show the intensity variations for the plane and the waveguide along $X - X'$ in Figs. 4(a)-(d) and 5(a)-(b). Figures 6(c) and (d) are those along $Y - Y'$ at x = 500 nm in Figs. 6(a) and (b), respectively. From the line profiles, we have found that the experimental results approximately fall between two calculated results. Furthermore, remarkable changes in SPP propagation properties between the two structures become apparent. For the Ag plane, SPP intensities attenuate monotonically without any intensity oscillation, which is also supported by eq. (4). Although small intensity fluctuations are observed along the *y* direction in Fig. 6(c), their cause has yet to be ascertained. For the Ag waveguide, however, the SPP intensities decay with oscillation whose period is similar to the computational result, as shown in Fig. 6(b). From Fig. 6(d), we can find the interference fringes more obviously. The larger damping for the experimental result in the plane is attributed not only to the uncertainty in the dielectric constant, but also to SPP scattering at the rough Ag surface. The ratio of the roughness to the excitation wavelength ($\delta/\lambda = 9.28 \times 10^{-3}$) is larger than in another report[20], 3.16×10^{-3}, and possibly has larger influence on SPP scattering at $\lambda = 405$ nm. However, the damping in the waveguide seems suppressed compared to the plane. To clarify the mechanism for this difference, we need to assess the dependence of SPP propagation properties on waveguide widths or an excitation wavelength.

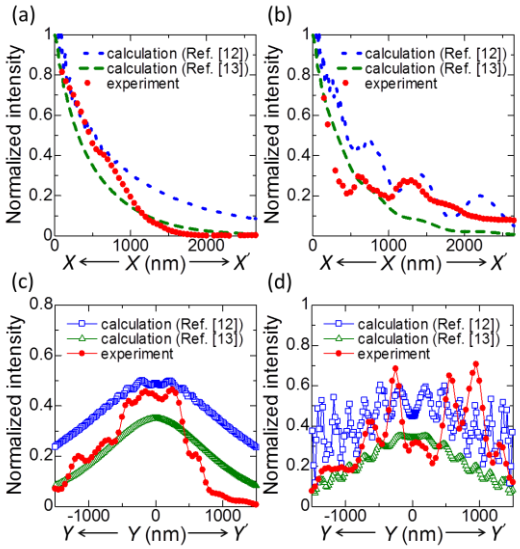

Fig. 6. (Color) (a) Intensity variation along $X - X'$ for the Ag plane in Figs. 4(a) (dashed line), 4(c) (dotted line), and 5(a) (circles). (b) As in (a) but for the Ag waveguide. (c) Intensity variation along $Y - Y'$ for the Ag plane in Figs. 4(a) (triangles), 4(c) (squares), and 5(a) (circles). (d) As in (c) but for the Ag waveguide.

5. Conclusions

We have visualized SPP propagation on two Ag waveguides using DSNOM. In the case of the plane structure with an infinite width, we have found that SPPs spread radially. In contrast, for the waveguide structure with a $3.4 - \mu m$ width, SPPs formed interference fringes, both along the propagation direction and perpendicular to it. By comparing the experimental and the FDTD results with two distinct dielectric constants as parameters, we found that the calculations using the value reported in ref. 13 were in good accordance with the experimental data. Therefore, we have demonstrated that our DSNOM clarifies the nanoscale behavior of SPP propagation.

Acknowledgment

Part of this study was supported by a Grant-in-Aid for Scientific Research from the Japan Society for the Promotion of Science. One of the authors (K.O.) acknowledges support from JST PRESTO.

References

[1] E. Kretschmann, H. Raether, Z. Naturforsch. 23A (1968) 2135.

[2] A. Otto, Z. Phys. 216 (1968) 398.

[3] B. Hecht, H. Bielefeldt, L. Novotny, Y. Inouye, D. W. Pohl, Phys. Rev. Lett. 77 (1996) 1889.

[4] Sergey I. Bozhevolnyi, Valentyn S. Volkov, Alexandra Boltasseva, Kristjan Leosson, Opt. Commun. 223 (2003) 25.

[5] I. I. Smolyaninov, D. L. Mazzoni, J. Mait, C. C. Davis, Phys. Rev. B 56 (1997) 1601.

[6] J.-C. Weeber, J. R. Krenn, A. Dereux, B. Lamprecht, Y. Lacroute, J. P. Goudonnet, Phys. Rev. B 64 (2001) 045411.

[7] R. Dallapiccola, C. Dubois, A. Gopinath, F. Stellacci, L. Dal Negro, Appl. Phys. Lett. 94 (2009) 243118.

[8] X. Ren, A. Liu, C. Zou, L. Wang, Y. Cai, F. Sun, G. Guo, G. Guo, Appl. Phys. Lett. 98 (2011) 201113.

[9] A. Kaneta, T. Hashimoto, K. Nishimura, M. Funato, Y. Kawakami, Appl. Phys. Express 3 (2010) 102102.

[10] J. Berthelot, F. Tantussi, P. Rai, G. Colas des Francs, J.-C. Weeber, A.Dereux, F. Fuso, M. Allegrini, A. Bouhelier, J. Opt. Soc. Am. B 29 (2012) 226.

[11] P. Berini, Phys. Rev. B 61 (2000) 10484.

[12] P. Berini, Opt. Express 7 (2000) 329.

[13] P. B. Johnson, R. W. Christy, Phys. Rev. B 6 (1972) 4370.

[14] D. W. Lynch, W. R. Hunter: in Handbook of Optical Constants of Solids, ed. E. D. Palik (Academic Press, New York, 1985) p. 275.

[15] U. Schröder, Surf. Sci. 102 (1981) 118.

[16] L. G. Schulz, J. Opt. Soc. Am. 44 (1954) 357.

[17] L. G. Schulz, F. R. Tangherlini, J. Opt. Soc. Am. 44 (1954) 362.

[18] G. B. Irani, T. Huen, F. Wooten, J. Opt. Soc. Am. 61 (1971) 128.

[19] B. Lamprecht, J. R. Krenn, G. Schider, H. Ditlbacher, M. Salerno, N. Felidj, A. Leitner, F. R. Aussenegg, J.-C. Weeber, Appl. Phys. Lett. 79 (2001) 51.

[20] A. Kolomenski, A. Kolomenskii, J. Noel, S. Peng, H. Schuessler, Appl. Opt. 48 (2009) 5683.